

Model-Based Qubit Noise Spectroscopy

Kevin Schultz,¹ Christopher A. Watson,¹ Andrew J. Murphy,¹ Timothy M. Sweeney,¹ and Gregory Quiroz^{1,2}

¹*Johns Hopkins University Applied Physics Laboratory, Laurel, MD 20723, USA*

²*William H. Miller III Department of Physics & Astronomy,
The Johns Hopkins University, Baltimore, MD 21218, USA*

Qubit noise spectroscopy (QNS) is a valuable tool for both the characterization of a qubit’s environment and as a precursor to more effective qubit control to improve qubit fidelities. Existing approaches to QNS are what the classical spectrum estimation literature would call “non-parametric” approaches, in that a series of probe sequences are used to estimate noise power at a set of points or bands. In contrast, model-based approaches to spectrum estimation assume additional structure in the form of the spectrum and leverage this for improved statistical accuracy or other capabilities, such as superresolution. Here, we derive model-based QNS approaches using inspiration from classical signal processing, primarily through the recently developed Schrödinger wave autoregressive moving-average (SchWARMA) formalism for modeling correlated noise. We show, through both simulation and experimental data, how these model-based QNS approaches maintain the statistical and computational benefits of their classical counterparts, resulting in powerful new estimation approaches. Beyond the direct application of these approaches to QNS and quantum sensing, we anticipate that the flexibility of the underlying models will find utility in adaptive feedback control for quantum systems, in analogy with their role in classical adaptive signal processing and control.

I. INTRODUCTION

Fault-tolerant error-corrected quantum computation offers the potential for more efficient computation in a number of problem domains, such as factoring of numbers using Shor’s algorithm [1–3], solving linear systems [4–7], quantum simulation and chemistry [8–12], and other areas [13–18]. Key to this fault tolerance are high-fidelity physical gates whose error-rates are below some threshold level, such that repeated layers of error correction can arbitrarily reduce logical error rates. Considerable research has been performed on reducing error sources present in a device (through, e.g., novel materials, process improvements, and circuit design [19–23]), as well as mitigating the impact of error sources using quantum control [24–30].

One particularly impactful application of quantum control is the reduction of semiclassical, time-correlated noise. This type of noise is widely present in physical systems [31–38]. In order to maximize the efficacy of quantum control, it is generally necessary to first characterize the noise environment, a process called qubit noise spectroscopy (QNS) [39–46]. These approaches can be interpreted through the lens of the filter function formalism [27, 47], which relates a given probe sequence to its filter function in the frequency domain, and the corresponding observable to the overlap of the filter function with the noise power spectrum. Many different probe sequences are then fed through the system, and the expectation values of the measured observables are jointly analyzed (typically through a form of least squares regression analysis) to estimate the power spectrum of the noise.

In the context of *classic* spectrum estimation, these QNS approaches closely resemble “nonparametric” spectrum estimation. These estimators can be interpreted as taking a collection of filters, applying them to the signal of interest, and analyzing the collective outputs as inner products (i.e., overlaps) to estimate the power spectrum [48]. Nonparametric approaches to spectrum estimation include the periodogram (squared magnitude of the (fast) Fourier transform of the sig-

nal), windowed and averaged periodograms (such as Bartlett’s [49] and Welch’s [50] methods), and the multitaper method [51] (c.f., the qubit control noise estimation considered in [43]).

In contrast, “parametric” or model-based approaches to noise spectroscopy [52, 53] assume a functional form (i.e., a model) and attempt to estimate the parameters rather than the spectrum directly. Model-based approaches offer statistical benefits over nonparametric approaches, such as reduced error variance (fewer parameters to estimate with the same data) and flexible approaches to model selection to reduce overfitting. Beyond these statistical benefits, we note that these model-based approaches produce estimates defined at all frequency points, as compared to the finite band resolution in nonparametric approaches, offering the potential for so-called superresolution.

Here, we adapt some common model-based approaches from classical noise spectroscopy, specifically autoregressive moving-average (ARMA) models and line spectra, to the QNS problem. In addition to direct adaptation of classical algorithms, such as Yule-Walker (YW) [54–56] and multiple signal classification (MUSIC) [57], we show how the recently introduced Schrödinger Wave ARMA (SchWARMA) model [58, 59] can be used to directly fit model parameters and how model-selection rules from classical spectrum estimation can be used to reduce overfitting and improve estimation accuracy. Beyond QNS, we note that these approaches may find applications in related problems in quantum sensing and control, c.f., the line spectrum signal model of Ref. [60], bandlimited signal model of Ref. [61], or control noise model of [62].

In this paper, Sec. II reviews QNS in the context of single-qubit dephasing noise, although we note that the approaches here should extend to arbitrary noise scenarios where filter-function based approximations remain valid, such as control noise [43], multi-qubit noise [42, 46], multi-axis noise [44], non-Gaussian noise [40, 45], and quantum noise [42]. In Sec. III, we formally introduce the most common models used in classical spectrum estimation and discuss how to adapt

common fitting algorithms to the QNS case, also introducing a flexible new approach based on the SchWARMA model. Next, in Sec. IV, we demonstrate the efficacy of model-based QNS using SchWARMA via simulation in white noise, bandlimited noise, and complex $1/f^\alpha$ -like spectra. We then consider experimental bandlimited noise injection data taken from Ref. [59] to further validate the SchWARMA-fitting approach. We then pivot in Sec. V to consider a different application of model-based QNS, where we show how our techniques are able to finely resolve spectral features using both simulated and experimental data. We conclude with discussion and potential future directions.

II. QUBIT NOISE SPECTROSCOPY

In this work, we are concerned with the estimation of a dephasing noise spectrum of a qubit, i.e., a qubit undergoing semi-classical noisy Hamiltonian dynamics governed by

$$H(t) = \eta(t)\sigma_z/2 + \Omega(t)\sigma_x/2 \quad (1)$$

where η is a zero-mean, wide-sense stationary Gaussian process and Ω is our single axis control signal. In this formulation, the role of $\Omega(t)$ is to define a series of noise probe sequences that can estimate the power spectrum $S_\eta(\omega)$ of η , i.e., the Fourier transform of the autocovariance $E[\eta(t_1), \eta(t_2)] = E[\eta(|t_1 - t_2|)\eta(0)] \triangleq r_\eta(t_1 - t_2)$.

The relationship between the control and the noise spectrum of the model in Eq. (1) can be interpreted through the filter function formalism [27, 47]. In the restricted setting of Eq. (1), we can associate with the control sequence $\Omega(t)$ a frequency domain representation $F_\Omega(\omega)$ of the control's impact on the dephasing noise and approximate the survival probability of a qubit prepared and measured in the $|+\rangle$ state by

$$p \approx \frac{1}{2} + \frac{1}{2} \exp\left(-\int d\omega S_\eta(\omega) F_\Omega(\omega)\right). \quad (2)$$

The quantity $\chi = \int d\omega S_\eta(\omega) F_\Omega(\omega)$ is often referred to as the *overlap integral* in the literature.

Eq. (2) suggests a method for estimating the power spectrum S_η by using different control sequences Ω_k to measure survival probabilities p_k and then “inverting” the relationship in (2). Since the left hand side of Eq. (2) is discrete, but $S_\eta(\omega)$ is continuous in ω , it is common to restrict the estimation to discrete frequency points ω_j . Assuming K total sequences and J total frequency points to be estimated, this sets up a system of equations

$$\chi_k \approx \sum_{j=1}^J F_{\Omega_k}(\omega_j) S_\eta(\omega_j) \quad (3)$$

where $\chi_k = \log(2(p_k - \frac{1}{2}))$ is measured experimentally. This can be expressed in matrix form as

$$\chi \approx \mathbf{F}\mathbf{S}, \quad (4)$$

which can be solved using some form of linear regression to recover an estimate $\hat{\mathbf{S}}$ of the power spectrum. Assuming

$J \geq K$ and \mathbf{F} is reasonably well conditioned, this can be solved using nonnegative least squares (NNLS) to recover an estimate $\hat{\mathbf{S}}$. Here, we consider the fixed total time pulse sequences (FTTPS) used in [58, 59], which are $X(\pi)$ -pulse sequences that result in spectral concentration at fixed intervals, thus $\omega_j = j\omega_*$ for some ω_* determined by the gate-duration and overall probe sequence length.

III. MODEL-BASED SPECTRUM ESTIMATION

In classical signal processing, spectrum estimation of a time series is a well-studied problem [48–53]. Fourier-analytic approaches to spectrum analysis date back at least as far as the late 19th century with the work of Schuster [63], who appears to have originally coined the term *periodogram* [64]. Unfortunately, a “raw” periodogram (that is, the square of the amplitudes of a discrete-time Fourier transform of a time series) does not reduce the variance of a spectrum estimate as the number of samples increases. Instead, techniques based on refining the periodogram, such as Blackman-Tukey’s, Bartlett’s, Welch’s, Daniell’s, and Thomson’s methods [53, Ch. 2], use some additional form of averaging and windowing (i.e., filtering) to produce statistically well-behaved estimates in a coarser set of frequency bands. All of these approaches are considered nonparametric, as they place no additional assumptions on the signal model (other than wide sense stationarity and Gaussianity) and can be directly interpreted as estimating the power in a set of frequency bands using a set of bandpass filters [48].

In contrast, methods that assume the signal satisfies a generating model with known functional form and attempt to estimate parameters of that model are referred to as parametric or model-based approaches [52, 53]. In the context of the filter-based viewpoint of nonparametric estimators [48], parametric estimators do not have to consider sidelobe or leakage effects that can impact the frequency concentration in the pass-band. These model-based approaches implicitly incorporate this model as additional information and can potentially offer statistical benefits over nonparametric estimators when the number of model parameters to be estimated is fewer than the number of nonparametric frequency bands required to achieve a desired spectral resolution. Additionally, model-based approaches offer natural options for model-selection [65] that reduce chances of overfitting.

A. Classical Methods for Model-Based Spectrum Estimation

There are a number of classical methods for spectrum estimation that fall under the designation of model-based estimates. Perhaps the most common approach to model-based spectrum estimation is to fit the time series in question to an ARMA model, which models a classical discrete-time series $y[k]$ via the linear combination of p prior values $y[k-i]$ and $q+1$ independent Gaussian inputs from the time series $x[k-j]$

via

$$y[k] = \underbrace{\sum_{i=1}^p a_i y[k-i]}_{AR} + \underbrace{\sum_{j=0}^q b_j x[k-j]}_{MA}, \quad (5)$$

which is denoted an $ARMA(p, q)$ model (for $p, q > 0$). When the model has $q = 0$, it is known as an $AR(p)$ (autoregressive of order p) model, and when $p = 0$ it is known as an $MA(q)$ (moving-average model of order q). An ARMA model results in a (discrete-time) power spectrum $S_y(\omega)$ for y of

$$S_y(\omega) = \frac{|\sum_{k=0}^q b_k \exp(-ik\omega)|^2}{|1 + \sum_{k=1}^p a_k \exp(-ik\omega)|^2}. \quad (6)$$

In other words, the ARMA approach assumes a rational polynomial form of the power spectrum, but this restriction is known to be dense in the space of valid power spectra [53] (periodic in 2π , as for discrete-time signals). Furthermore, this density property holds for pure AR and MA models as well.

Another model common in the classical literature is to assume that the signal has a *line spectrum*, that is, the signal $y(t)$ is a sum of sinusoids (the signal $x(t)$) in the presence of additive noise $e(t)$:

$$y(t) = \underbrace{\sum_{k=1}^n A_k \exp(i(\zeta_k t + \phi_k))}_{x(t)} + e(t), \quad (7)$$

where A_k , ζ_k , and ϕ_k are the unknown (to be inferred) amplitude, frequency, and phase, respectively, of the k th sinusoid. We note that for the purposes of power spectrum estimation, the phases are irrelevant. Generally, n is assumed to be specified or otherwise selected based on the data (as with the ARMA model orders p and q , above), and $e(t)$ is generally assumed to be white Gaussian noise.

B. Adaptation to QNS

Unlike the classical case, where one would have access to the complete time series, in the QNS setting we have access to only some collection of sample average values. Via the filter function formalism, we see that this is approximately the average of the overlap between the control signal's filter "power" and the dephasing noise spectrum. In this sense, conventional QNS approaches most closely resemble the quadratic estimator viewpoint of classical filtering/windowing-based methods [48], albeit with constraints on the available forms of the filter to be used.

To overcome this limitation, we propose two different methods for adapting these classic model-based approaches to the quantum setting. The first approach is to estimate, using NNLS QNS, the noise power spectrum \hat{S}_η , or equivalently via Fourier transform the autocovariance \hat{r}_η . The spectrum can

then be used to produce model-based spectrum estimates via approaches that do not require access to the time series itself, such as YW approaches to AR models. The second option, which applies to general (i.e., AR-, MA-, or ARMA-based) models, is to exploit the differentiability of Eqs. (6) and (2) using the recently introduced SchWARMA model [58].

C. Spectrum Estimation Using \hat{r}_η

Using the NNLS approach to spectrum estimation, one can produce an estimate $\hat{S}_\eta(\omega_j)$ at the discrete frequencies ω_j . By applying the inverse discrete-time Fourier transform to \hat{S}_η , we can obtain an estimate of the discrete-time autocovariance function $\hat{r}_\eta(t_j)$. Classically, many parametric techniques for discrete-time power spectrum estimation are derived from the autocovariance, as it is a trivial calculation to estimate the variance between a time series and time-lagged versions of itself. In particular, there are ways to estimate the coefficients of an ARMA model from \hat{r}_η (as opposed to e.g., maximum likelihood methods that rely on samples of the time-series directly). We will briefly review a few of these approaches that we have currently implemented in our software toolbox, *mezze* [66].

The first approach we will consider is the adaptation of the YW equations for estimating $AR(p)$ models to the QNS setting. Classically, the autocovariance r_y of the sequence y_k can be estimated using direct empirical averaging of $\hat{r}_y[k] = \frac{1}{N-j} \sum_{k=0}^{N-j-1} y[k]y[k+j]$ or, more computationally efficiently for large N , repeated application of the fast Fourier transform. Regardless of the specific method used, it is clear that this is not possible in the QNS context, as we do not have direct access to discrete-time samples of the noise process η . Instead, we will use the Fourier transform of the NNLS estimate \hat{S}_η to produce an estimate $\hat{r}_\eta[k]$. The YW approach for QNS then proceeds in the usual fashion by first solving for a_1, \dots, a_p using the Toeplitz autocovariance matrix $\hat{\mathbf{R}}$

$$\begin{bmatrix} \hat{r}_\eta[1] \\ \hat{r}_\eta[2] \\ \vdots \\ \hat{r}_\eta[p] \end{bmatrix} = \underbrace{\begin{bmatrix} \hat{r}_\eta[0] & \hat{r}_\eta[1] & \hat{r}_\eta[2] & \cdots \\ \hat{r}_\eta[1] & \hat{r}_\eta[2] & \hat{r}_\eta[3] & \cdots \\ \hat{r}_\eta[2] & \hat{r}_\eta[3] & \hat{r}_\eta[4] & \cdots \\ \vdots & \vdots & \vdots & \ddots \\ \hat{r}_\eta[p-1] & \hat{r}_\eta[p-2] & \hat{r}_\eta[p-3] & \cdots \end{bmatrix}}_{\hat{\mathbf{R}}} \begin{bmatrix} a_1 \\ a_2 \\ a_3 \\ \vdots \\ a_p \end{bmatrix} \quad (8)$$

in the least squares sense. Next, the sole remaining unknown in the $AR(p)$ model b_0 can be solved by noting that $\hat{r}_\eta[0] = \sum_{k=1}^p a_k \hat{r}_\eta[k] + b_0^2$, and noting that the sign of b_0 is irrelevant in the power spectrum in Eq. (6). In addition to this form of YW, we will also take advantage of the fact that we will always have N time estimates for \hat{r}_η (i.e., in contrast with the classical case, we do not have the option of estimating *only* the first p time lags); we can instead consider the overdetermined set of equations by using the first p columns of $\hat{\mathbf{R}}$ and adapting Eq. (8) accordingly. A brief discussion on the implications of using an overdetermined YW fit can be found in [53, Sec. 3.7.1].

Unfortunately, MA models cannot be cast in a similar linear regression problem. Instead, we will exploit the fact that an $MA(q)$ model

$$y[k] = \sum_{j=0}^q b_j x[k-j] \quad (9)$$

satisfies $r_y[k] = \sum_{j=k}^q b_j b_{j-k}$, which in particular implies that the autocovariance of y vanishes after q time lags. Minimization of the function $\sum_{k=0}^q (\hat{r}_\eta[k] - \sum_{j=k}^q b_j b_{j-k})^2$ can be solved using Newton's method or some other form of gradient descent from a suitable initial condition (here $b_0 = \hat{r}_\eta[0] + 2 \sum_{j=1}^q \hat{r}_\eta[j]$, $b_j = 0$ for $j > 0$) [67]. This method converges sufficiently rapidly and accurately for our purposes, but other methods for the design of MA models can be found in the filter design literature [68].

For the fitting of full $ARMA(p, q)$ models, we turn to the cepstrum (log of the power spectrum) recursion techniques of Ref. [69]. The first step in this approach is to estimate the $AR(p)$ portion of the model using the (overdetermined) YW approach as described above. Defining the cepstrum as the inverse Fourier transform of the log of the power spectrum determined from the NNLS estimate, $\hat{c}(\omega_k) = \mathcal{F}^{-1}\{\log(\hat{S}_\eta(\omega_k))\}$, the normalized coefficients b'_k can be estimated recursively by setting $b'_0 = 1$ and for increasing k (up to $k = q$) via

$$b'_k = \frac{1}{k} \left[k \hat{c}_k b'_0 - \sum_{m=1}^{k-1} m b'_m a_{k-m} + \sum_{m=1}^k m a_m b'_{k-m} + \sum_{j=1}^{k-1} j \hat{c}_j \sum_{m=0}^{k-j} a_m b'_{k-j-m} \right]. \quad (10)$$

The above MA coefficients are ‘‘accurate’’ up to an overall scale factor κ^2 which can be determined from the ratio between the NNLS estimate and the ARMA power determined by $\{a_k\}$ and $\{b'_k\}$. We further optimize κ^2 by finding the minimum mean squared error between the corresponding filter function predictions and the observed outcomes. We then set the actual MA estimates by $b_j = \kappa b'_j$.

With respect to line spectra, a common approach to spectrum estimation is to fit the spectrum using an $AR(p)$ model [53]. Under this model, the complex zeros of the denominator in the rational power spectrum (the so-called ‘‘poles’’ of the AR model) will presumably match the frequencies of the line spectrum (i.e., their complex argument corresponds to the normalized frequency) and the power at that frequency determines the amplitude of that sinusoidal component. In the QNS context, this approach can be estimated using the same YW adaptation as above.

Beyond the ARMA family, there are fundamentally different model-based methods for line spectrum estimation that use estimates of the autocovariance, and here we will consider MUSIC [57]. Unlike ARMA-based approaches which assume a rational polynomial form of the power spectrum, MUSIC generalizes Pisarenko's method [70] and instead assumes that the unknown signal is a linear combination of a

known number of complex exponentials corrupted by additive white Gaussian noise. The first step in a MUSIC approach to QNS is to again compute an estimate of autocovariance matrix \hat{R} . Since \hat{R} is symmetric, it admits the eigendecomposition $\mathbf{V}\mathbf{\Lambda}\mathbf{V}^\top$, where \mathbf{V} is orthogonal (i.e., real-valued and unitary), and $\mathbf{\Lambda}$ is a diagonal matrix of nonnegative eigenvalues λ_i , with $\lambda_1 \geq \lambda_2 \geq \dots \geq \lambda_J \geq 0$. Under the assumption that η consists of p complex exponentials, MUSIC first defines a ‘‘pseudo-spectrum’’ by

$$\hat{S}_{MU}(\omega) = \frac{1}{\sum_{i=p+1}^J |e^\dagger(\omega)\mathbf{V}_i|^2}, \quad (11)$$

where \mathbf{V}_i denotes the i th column of \mathbf{V} and $e(\omega) = (1, e^{i\omega}, e^{i2\omega}, \dots, e^{i(J-1)\omega})^\top$, a frequency vector. Next, the p largest local maxima of \hat{S}_{MU} (between 0 and π) are determined numerically and set as the (normalized) frequencies of the p complex exponentials assumed to compose the signal.

D. Model Based Spectrum Estimation Using SchWARMA

The SchWARMA approach introduced in [58] and experimentally verified in [59] provides a link between classical ARMA models and noisy quantum circuits. In the restricted setting of Eq. (1), the continuous-time dynamics are replaced by a noisy discrete-time circuit with propagator

$$U(KT) = \prod_{k=1}^K Z(y[k])X \left(\int_{(k-1)T}^{kT} dt \Omega(t) \right), \quad (12)$$

where K is the number of gates in the noiseless circuit, T is the gate time, $y[k]$ are the outputs of a classical ARMA model as in Eq. (5), and $Z(\theta)$ and $X(\theta)$ are Z and X rotation gates, respectively. Assuming the resulting $X(\theta)$ have $\theta \in \{0, \pi\}$ (as in the FTTPS), the resulting filter function computation of Eq. (2) is exact in the instantaneous control limit.

Given the results $\{p_k\}$ of some dephasing QNS experiment, we can attempt to either fit an ARMA model using the methods described above, and thus produce a SchWARMA model, or to fit the SchWARMA model directly to the data p_k without first performing an NNLS power spectral density (PSD) estimate. To achieve the latter, we note that the survival probabilities p_k are differentiable with respect to the SchWARMA model parameters a_i and b_j , as the power spectrum in Eq. (6) is differentiable with respect to the model parameters and Eq. (2) is differentiable with respect to the power spectrum. Thus, the SchWARMA-based prediction \hat{p}_k of a given QNS probe sequence using Eqs. (6) and (2) are differentiable with respect to the SchWARMA model parameters. Given a differentiable loss function $L(\{p_k\}, \{\hat{p}_k\})$ of the true and predicted survival probabilities (such as $\sum_k (p_k - \hat{p}_k)^2$), it is possible to use gradient descent to minimize this loss. To this end, we use TensorFlow's autodifferentiation [71] and its implementation of the ADAM optimizer [72] to minimize the mean squared error of the predictions.

IV. SPECTRUM ESTIMATION

In this section, we investigate the SchWARMA approach to spectrum estimation in a variety of scenarios, using both simulated and experimental data. We chose to focus only on the SchWARMA approach as we generally found it to be more accurate from random initial conditions than the adaptations using the NNLS-derived autocovariance. Furthermore, the differentiability of the SchWARMA approach ensures that it can improve (in a mean-square error sense) initial models estimated using those approaches. To this end, we use the cepstrum-based estimates as our initial conditions for the SchWARMA fits and this generally outperforms random initial conditions, especially for complex models. Additionally, the SchWARMA approach is less reliant on the conditioning of the NNLS-based regression problem and could potentially be used in conjunction with probe sequences that are not otherwise suited to effective QNS, although we leave this investigation to future work. However, the SchWARMA approach does add computational and time overhead to computing an estimate, and it is possible that there are real-time QNS problems that could benefit from the other adaptations. In these cases, we recommend the cepstrum-based approach as it fully subsumes the Yule-Walker approach for purely autoregressive models and scales much better for moving average models than the pure-optimization approach described above.

A. White Noise

A simple example that highlights the difference between standard NNLS-based spectrum estimation and model based approaches occurs when the dephasing noise spectrum comprises only white noise. In this case, the overlap integral in Eq. (2) will be constant for each sequence in the FTTPS, since their total time is the same. In the infinite measurement limit, we would therefore expect the survival probabilities to be the same; however, when the measurements are finite, there will be variance in the empirical survival probabilities due to the underlying binomial distribution, as in Fig. 1a. When these survival probabilities are inverted using NNLS we see similar variation in the estimated power in each band, as shown in Fig. 1b.

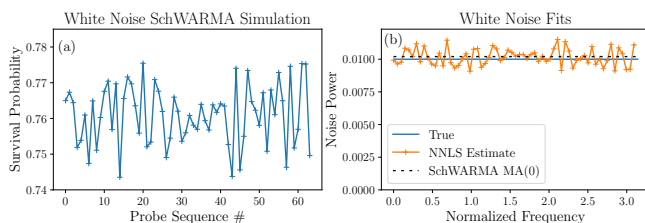


FIG. 1. Simulated QNS experiment of white noise. (a) Simulated FTTPS survival probabilities using 1000 SchWARMA trajectories; note the variability due to the binomial measurement distribution. (b) True and estimated noise spectra.

In contrast, a model-based approach using a SchWARMA

model is able to more accurately estimate the true spectrum. Since white noise is equivalent to an $MA(0)$ model (and indeed these simulations were performed using an $MA(0)$ SchWARMA model), we should in principle be able to accurately estimate the spectrum using a model of the same form. When we fit a SchWARMA model directly to the simulated QNS experiment, we see that the power spectrum is flat and also quite accurate (see Fig. 1b), here estimating the noise power within $\approx 0.7\%$. This simple example illustrates a potential benefit of model-based spectrum estimation. As there are now fewer model parameters than probe sequences, the experimental data is effectively “pooled,” reducing estimation error. To further demonstrate how this works, when we simply take the average survival probability across all probe sequences, we find that the estimated power spectrum from that average is comparable (sometimes better, sometimes worse) to the SchWARMA estimate.

We note that in this case, the SchWARMA fit is somewhat unnecessary, since it is fairly obvious that the spectrum in Fig. 1 is quite flat, and one would be inclined to fit a horizontal line to the resulting NNLS estimates to determine the white noise power. A similar approach is often used in the fitting of $1/f^\alpha$ spectra to QNS experiments, whether the underlying estimates come from FTTPS sequences [59] or other probe approaches [32, 39, 42, 43].

B. Time-Correlated Noise

To illustrate model-based spectrum estimation on more complex noise models, in this section we consider two different correlated noise spectra. These are 1) a bandlimited noise spectrum, modeling the noise injection experiments of [59] and 2) a complex noise spectrum generated by the sum of $1/f^2$ noise, a wide bandlimited region, and two narrow spectral features. Simulated FTTPS QNS results for these two noise models are shown in Fig. 2a and b, respectively. Noise reconstructions for the bandlimited case are shown in Fig. 2c, and two different views for the complex spectrum are shown in Fig. 2d and e.

For the NNLS noise estimates, we performed cubic spline interpolation to produce spectrum estimates that are continuous in frequency, as opposed to the discrete point estimates naturally produced by the least-squares inversion process, in order to provide a more fair comparison between approaches. Additionally, we found that cubic spline interpolation produced better results than lower-order spline interpolation and Fourier (sinc)-based interpolation. We compare the accuracy of these two approaches later in this section, but for now we note that the spectral leakage of the filter functions in the NNLS appear to result in slightly narrower estimates of the passband region at the top along with slightly wider estimates at the bottom, as shown in Fig. 2c and e. Similarly, the NNLS method appears to underestimate the peak of the spectral features in Fig. 2d to a greater degree than the SchWARMA approach.

As suggested in the previous section, a powerful property of ARMA models that SchWARMA models inherit is the abil-

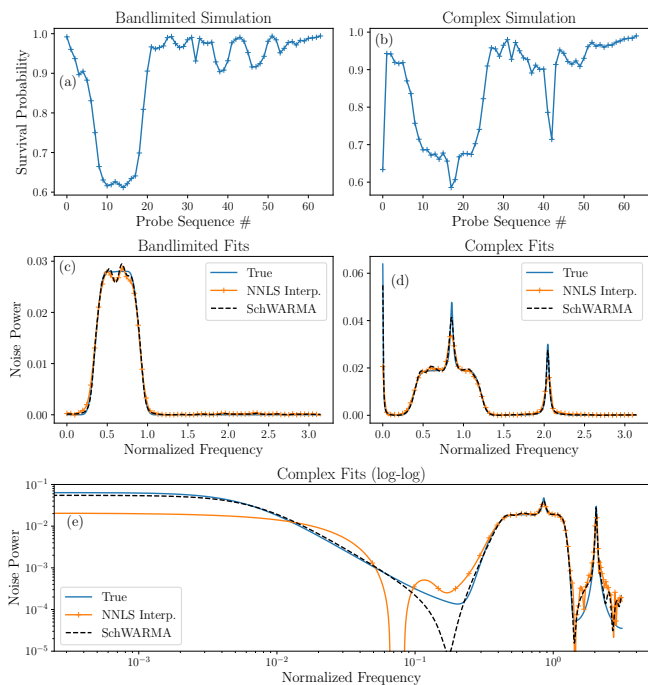


FIG. 2. SchWARMA simulations and spectral reconstructions for correlated noise spectra. (a) Simulated QNS experiments of the bandlimited noise spectrum. (b) Simulated QNS experiments of the complex noise spectrum formed by $1/f^2$ with additional spectral features. (c) Bandlimited noise spectrum and estimated spectra using the NNLS and SchWARMA approaches. (d) Complex noise spectrum and estimated spectra using the NNLS and SchWARMA approaches. (e) Same spectra as in (d), plotted on a log-log axis to better show the $1/f^2$ portion of the spectrum.

ity to perform model selection, meaning the ability to select p and q in a way that balances error with overfitting [65]. Here, we will consider two procedures for model selection, Akaike information criterion (AIC) and Bayesian information criterion (BIC). When applied to (linear) regression problems, these approaches penalize some function of the log-likelihood in terms of the mean-squared error (MSE) $1/K \sum_k (p_k - \hat{p}_k)^2$ of the fit residuals with a term that is dependent on the overall number of parameters (here $p + q + 1$). Specifically, for this QNS application, the AIC of a SchWARMA model is $K \log(MSE) - 2(p + q + 1)$, and the corresponding BIC is $K \log(MSE) - (p + q + 1) \log(K)$. Thus, the only difference between these two criteria is the way in which they penalize the number of parameters in the model.

To demonstrate and assess model selection while also validating SchWARMA model-based QNS, we performed 25 independent QNS simulations of FTTPS probe sequences under SchWARMA-driven dephasing noise for each of the two noise classes. We considered both 1000 and 10000 measurement shots per probe sequence to assess the influence of binomially distributed measurement error on the results. We computed the NNLS estimate for each QNS simulation, then interpolated them to get a continuous estimate to compare to the true power spectrum. Similarly, we fit SchWARMA mod-

els for each (p, q) pair such that $p + q + 1 \leq 64$ (the number of probe sequences). For each (p, q) , we computed the MSE between the SchWARMA predictions and the simulated data, along with the AIC and BIC. We then selected the model that produced the minimum MSE, AIC, and BIC and computed their spectrum reconstruction error. Box plots of the spectrum error distributions are shown in Fig. 3.

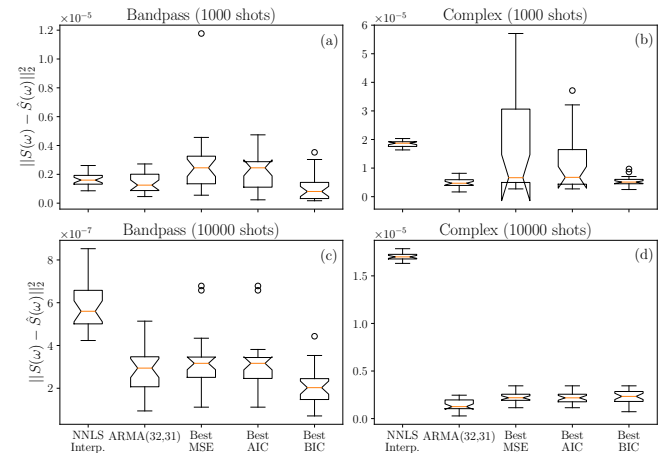


FIG. 3. Boxplots (25 independent simulations) of spectrum reconstruction error for interpolated NNLS, SchWARMA fit $ARMA(31, 32)$ models, and model-selected SchWARMA models using minimum mean squared error, Akaike information criterion, and Bayesian information criterion. (a) Bandpass noise, 1000 shots per probe sequence. (b) Complex spectrum, 1000 shots per probe sequence. (c) Bandpass noise, 10000 shots per probe sequence. (d) Complex spectrum, 10000 shots per probe sequence. Notches on the boxplot indicate 95% confidence in differences between medians if they do not overlap. Additionally, Wilcoxon signed-rank test indicates statistically significant differences between the NNLS-interpolated estimates and the SchWARMA-fit $ARMA(32, 31)$ and best BIC selected models for each case.

The results of this Monte Carlo analysis demonstrate that using minimum BIC as a model selection criterion outperforms the interpolated NNLS reconstructions in a statistically significant manner (Wilcoxon signed-rank test, $\max \alpha < 0.0004$ across the four scenarios), in contrast to using the minimum MSE or AIC as a selection criteria, which performed poorly on some of the 1000 shot trials. This is consistent with the general theory of model selection, as we expect BIC to more accurately estimate the number of parameters in a model [65].

We also recognize that some potential use cases of SchWARMA model-based QNS may not be amenable to exhaustive search over the range of valid (p, q) choices, if, for example, it is being used as part of a fast adaptive control loop. To this end, we also include the $ARMA(32, 31)$ model as a candidate that should exhibit flexibility in spectral structure with its mix of terms while also having the maximum number of parameters (here 64) in order to produce good fits. We find that this choice also outperforms the interpolated NNLS method in reconstructing the true spectrum (Wilcoxon signed-rank test, $\max \alpha < 0.05$), with comparable performance to

minimizing the BIC.

C. Native and Injected Experimental Noise in a Superconducting Qubit

In Ref. [59], a SchWARMA-based scheme for experimental dephasing noise was introduced. In that work, it was demonstrated that SchWARMA could accurately predict survival probabilities of QNS experiments given a native noise model and a desired injected spectrum. In this section, we use the experimental data from Ref. [59] to demonstrate the applicability of the model-based spectrum estimation techniques to real experimental data. This effectively ‘‘closes the loop’’ on SchWARMA as a noise simulation, injection, and estimation protocol. Fig. 4 shows bandlimited signal injected from Ref. [59], along with various SchWARMA predictions.

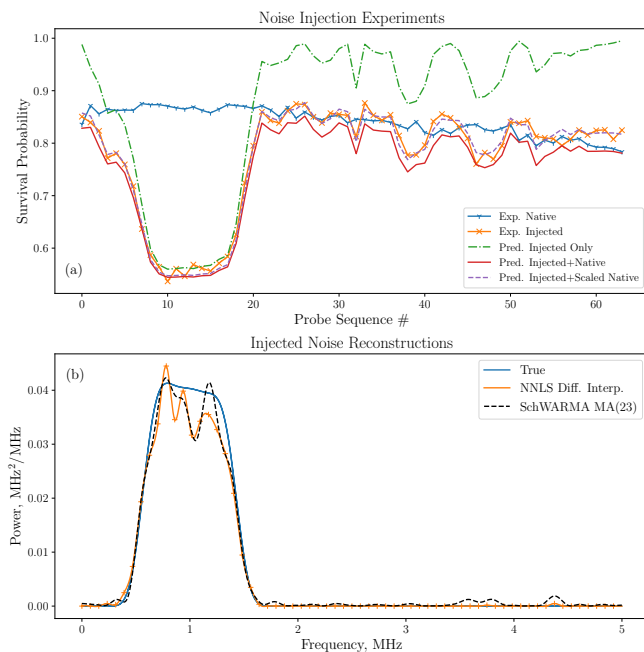


FIG. 4. Analysis of noise injection experiment from Ref. [59]. (a) Survival probabilities of FTTPS probe sequences with native and bandlimited injected (SDR-based) noise from Ref. [59], along with the SchWARMA-based predictions that incorporate only the injected noise power, the sum of the injected noise power with a native noise fit, and the sum of the injected noise power with a scaled noise fit to account for native noise fluctuation observed in the data. (b) Comparison of the true injected noise spectrum to an NNLS-based method derived by subtracting and truncating the native noise NNLS estimate, and the BIC-optimal SchWARMA fit that includes a scaled native noise.

Clearly, the predictions of the injected noise by itself do not come particularly close to capturing the behavior of the combined native and injected signal, due to the strength of the native noise. To resolve this, we can first perform a SchWARMA estimate of the native noise spectrum, $S_{nat}(\omega)$, then attempt to estimate only the injected noise spectrum, $S_{inj}(\omega)$, by replacing $S_{\eta}(\omega)$ in Eq. (2) with the sum $S_{nat}(\omega) + S_{inj}(\omega)$.

The native noise overlap term $-\int d\omega S_{nat}(\omega)F_{\Omega}(\omega)$ effectively behaves as a constant term in the SchWARMA model optimization process, allowing for the fitting to proceed in essentially the same manner as before. When we account for the native noise spectrum in this manner, for *this specific* experimental data, it appears that there has been some drift between the FTTPS experiments for native and injected QNS. This is evident in the lower survival probability predictions for the combination of estimated native noise and true injected noise, especially outside the band of the injected signal, indicating an overestimation of the combined noise sources. To account for this variation and truly demonstrate the predictive power of SchWARMA, we again use numerical optimization to find a native noise scale factor β such that the sum of the known injected spectrum and a scaled estimate of the native noise $\beta S_{nat}(\omega)$ minimizes the MSE of the filter function predictions of the survival probability. Predicted survival probabilities of this combination of injected and scaled native noise are also shown in Fig. 4a, and quite accurately predict the experimental results outside of the band of the injected signal.

With an accurate estimate of the native noise spectrum, we are now able to repeat the SchWARMA fit using the scaled native noise. The actual injected power spectrum and the estimated injected power using the scaled native noise are shown in Fig. 4b. For reference, we also computed a truncated difference between the NNLS estimates for the injected and native cases, setting all negative values to zero. We note that it is (presumably) by pure chance that the native noise power decreased for the injection experiments, and this leads to a zero power outside of the injected band for the NNLS reconstruction. If the situation were reversed, we would see spurious features in out-of-band portion of the estimated spectrum.

One interesting feature that we leave for future investigation is that the SchWARMA model selection approach using BIC drastically favors $AR(63)$ and $MA(64)$ models (i.e., the number of parameters are the same as the data size), for both the native and injected experimental data. This may be due to any number of reasons, including non-stationary fluctuations in the native noise and non-uniform accumulated gate error due to the differing number of X gates in the FTTPS sequences (as observed in Ref. [59]). However, when we incorporate the scaled native spectrum information in the fit to the injected signal, we do find that an $MA(21)$ model minimized BIC (which was used for the reconstruction in Fig. 4).

V. SUPERRESOLUTION

As discussed above, NNLS-based QNS fundamentally estimates the power spectrum in a set of power bands, whereas the model-based approaches estimate the power (or presence of signal for MUSIC) at individual frequencies. Thus, these model-based QNS approaches exhibit a phenomenon known as superresolution, where they are able to resolve spectral features at a finer scale than would be implied by the effective Nyquist rate. Fig. 5a shows SchWARMA-simulated survival probabilities of FTTPS dephasing spectrum with a peak between two NNLS bins. Note that this noise spectrum produces

a considerable drop in survival probability for two adjacent probe sequences.

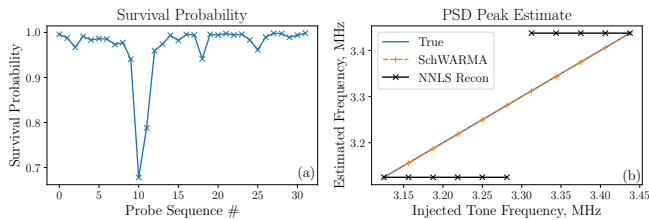


FIG. 5. (a) Simulated FTTPS QNS experiment of an incoherent tone modeled by an $AR(2)$ model with a peak between two FTTPS peak frequencies. (b) Frequency sweep of spectral peak and comparison of SchWARMA $AR(2)$ fit and NNLS peak.

Fig. 6 shows spectrum estimates of this peaked spectrum using several different estimation approaches. As expected, the NNLS reconstruction estimates considerable power in the two bands nearest the true center frequency. Using the NNLS estimate to produce a Yule-Walker $AR(2)$ estimate results in a spectrum estimate that is not particularly accurate with respect to either the overall power or the peak center frequency. In contrast, the MUSIC estimate using the same NNLS reconstruction has an accurate estimate of the peak's center frequency. However, as noted above, the MUSIC estimate only produces a pseudo-spectrum from which the noise's constituent harmonic components can be estimated. From Fig. 6 we see that this pseudo-spectrum is not suitable for estimating the overall power spectrum. Finally, a directly fit SchWARMA $AR(2)$ model produces a spectrum estimate that is extremely accurate to the true noise spectrum in terms of both the overall spectrum and the center frequency of the peak.

In the quantum context as with classical superresolution, these techniques function in the presence of multiple peaks (see Fig. 7). As before, the NNLS-based estimates have spectral concentration in pairs of adjacent bands, and this appears to bias both the Yule-Walker and MUSIC approaches. Additionally, we observed that we had to increase the number of parameters in the Yule-Walker and SchWARMA AR fits in order to produce a spectral estimate that results in two peaks (here $AR(12)$ was used). When the SchWARMA fits produce two peaks, the center frequencies of the peaks are quite accurate to the true center frequencies, although the overall power is not as accurate as the single peak case.

A. Experimental Validation

Fig. 8 shows the results of an experimental demonstration of superresolution using SchWARMA as compared to NNLS reconstructions. For these experiments, we injected a spectral peak (itself generated by an $AR(2)$ model) with center frequency between 0-5 MHz in 31.25 kHz increments, one fifth the resolution of the FTTPS-based NNLS approach. This signal was injected into our superconducting transmon qubit system using the software-defined radio-based approach of Ref. [59]. To identify the center frequency of the injected

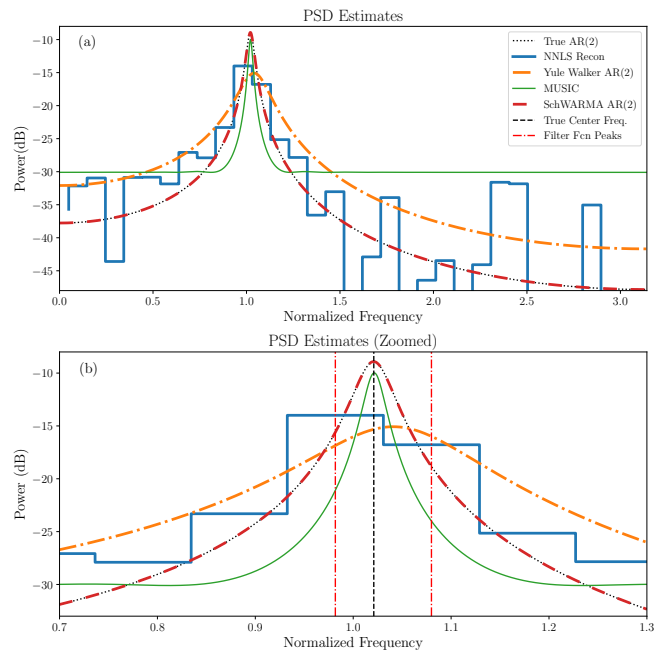


FIG. 6. Spectrum estimation of a spectral peak from the simulation in Fig. 5a. (a) Spectrum estimates over the full frequency range. (b) Zoomed view of spectrum estimates, with vertical lines indicating true center frequency (—) and peaks of the adjacent probe sequences (—).

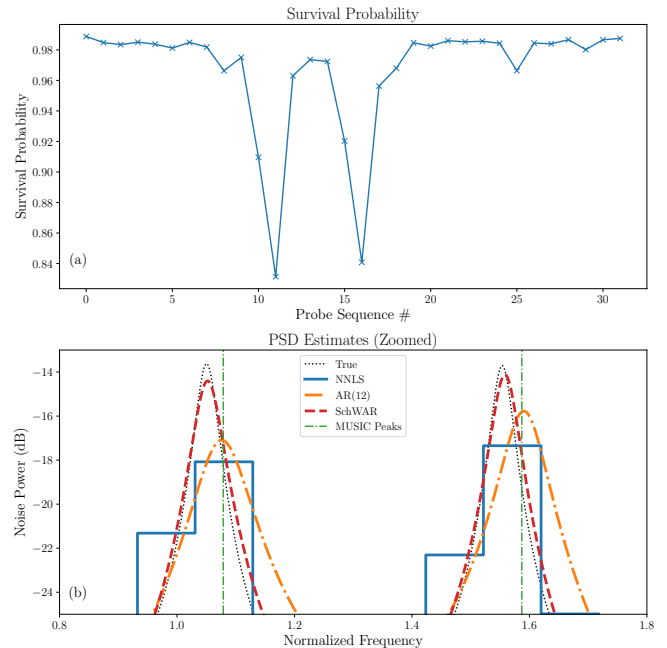


FIG. 7. Superresolution of a multiple-peak spectrum. (a) FTTPS survival probability simulation. (b) Comparison of different spectrum estimates to the survival probability data from (a).

peak, we first performed QNS of the native noise using each approach, then identified either the bin (for NNLS) or frequency (for SchWARMA) that exhibited the biggest increase

when the additional noise was injected. For both spectrum estimation approaches, we see considerable distortion at the extremes of the frequency range. For low frequencies, we conjecture that this is due to fluctuations in the $1/f^\alpha$ component of the native noise spectrum, which is dominant at low frequencies. For the higher frequencies, this appears to be an artifact of the noise injection approach, whose output power (as measured by the survival probability of the qubit) drops off noticeably at higher frequencies. Despite these limitations, we see that both approaches track the predicted FTTPS peak for a wide frequency range, and that the SchWARMA approach is more accurate to the injected peak. We note that finite measurement effects as well as fluctuations in the native noise are likely the limiting factors in the overall accuracy of the SchWARMA superresolution estimates.

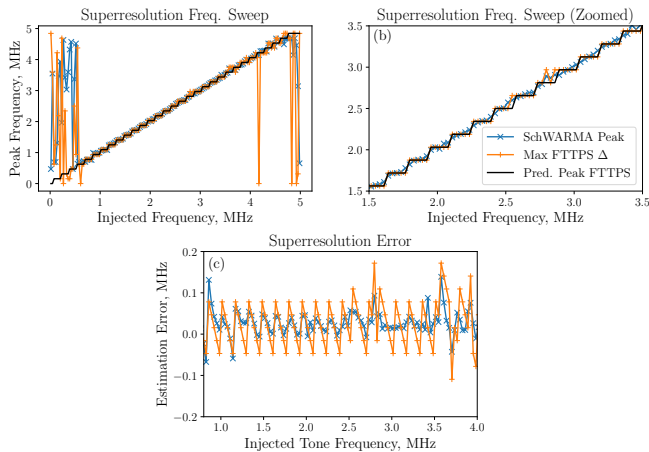


FIG. 8. Experimental superresolution results of an injected spectral peak. (a) Full sweep of peak center frequency from 0-5 MHz in 31.25 kHz increments. (b) Zoomed in view. (c) Error of peak estimates of SchWARMA and NNLS reconstructions.

VI. CONCLUSION

In conclusion, we have adapted a number of different model-based approaches for classical spectrum estimation to the field of QNS, demonstrating their efficacy in several scenarios using both simulation and experimental data. Specifically, we showed that SchWARMA-based estimators produced more accurate power spectra than NNLS-based estimators and that model-selection using BIC can be used to reduce the impact of overfitting. Additionally, we showed that SchWARMA can resolve much finer spectral features than NNLS-based estimation. Finally, we “closed” the SchWARMA modeling and estimation loop, verifying that the SchWARMA model is an effective model for noise simulation, injection, and estimation. Thus, the use of SchWARMA as a spectral model offers several potential benefits over standard NNLS approaches to QNS, and we have only scratched the surface of potential adaptation of classical time-series analysis to the QNS domain. We further note that one especially parsimonious use of the SchWARMA approach to

model-based QNS is that the resultant SchWARMA model can immediately be used as a generative model of the noise in a quantum system, through which the impacts of the noise on various circuits can be explored as in [58, 73] or used directly in model-based optimal control protocols [62].

Several of the model-based QNS approaches we considered are derived directly from a traditional non-parametric NNLS estimate of the spectrum, as the limitations of quantum mechanics prevent the direct computation of the noise autocovariance. While these approaches still have utility despite the dependence on the NNLS estimator, they are fundamentally limited by the statistical properties of that estimator, in particular the conditioning of the inversion matrix, which is ultimately determined by the probe sequences used. The FTTPS have excellent conditioning, but the number of sequences required (and their gate length) also scales linearly with the desired frequency resolution. In contrast, direct estimation of an underlying SchWARMA model is more flexible and could potentially produce useful, reduced order estimates despite ill-conditioning of the probe sequences used. Furthermore, it should be possible to extract spectrum information from characterization experiments not generally designed for spectrum estimation, such as randomized benchmarking [74] or gate set tomography [75]. Since model-based spectrum estimation is ultimately about the number of model parameters to be estimated, the number of probe sequences required for accurate estimation should be on the order of the number of model parameters, and not the desired frequency resolution. Additionally, there is the obvious potential for compressive sensing-like algorithms that can use a few random sequences to extract meaningful spectral information.

With regard to the experimental noise-injection data, the primary focus was demonstrating that the SchWARMA fitting approach can work with real experimental data, and indeed, we showed that we could find models that agreed with the survival probabilities up to numerical precision. However, it is likely that there are some non-dephasing noise sources that are also impacting survival probabilities, such as T_1 decay and gate-error, and a more complicated model would be required to discriminate between them. These unmodeled effects could also explain why the model-selection criteria tend to favor high parameter counts. Furthermore, the noise injection and native noise scenario is somewhat contrived in that we “know” the injected signal. In a more realistic quantum sensing scenario focused on signal detection as in [61], we can envision a system that continuously performs QNS and then tests the hypothesis that the native noise has changed or been rescaled against the possibility that an anomalous signal has been “injected” or is otherwise present in the system. In this case, we feel that the model selection rules and other statistical tools that operate on candidate models will lead to effective solutions, as classical ARMA models do in adaptive and statistical signal processing [76].

DATA AVAILABILITY

Python implementations of the model-based QNS routines are available at <https://github.com/mezze-team/mezze>.

ACKNOWLEDGEMENTS

KS and GQ acknowledge funding from ARO MURI grant W911NF-18-1-0218. GQ acknowledges funding from the

U.S. Department of Energy (DOE), Office of Science, Office of Advanced Scientific Computing Research (ASCR), Accelerated Research in Quantum Computing program under Award Number DE-SC0020316.

-
- [1] P. W. Shor, Algorithms for quantum computation: discrete logarithms and factoring, in *Proceedings 35th annual symposium on foundations of computer science* (IEEE, 1994) pp. 124–134.
- [2] I. L. Chuang, R. Laflamme, P. W. Shor, and W. H. Zurek, Quantum computers, factoring, and decoherence, *Science* **270**, 1633 (1995).
- [3] P. W. Shor, Polynomial-time algorithms for prime factorization and discrete logarithms on a quantum computer, *SIAM review* **41**, 303 (1999).
- [4] A. W. Harrow, A. Hassidim, and S. Lloyd, Quantum algorithm for linear systems of equations, *Phys. Rev. Lett.* **103**, 150502 (2009).
- [5] B. D. Clader, B. C. Jacobs, and C. R. Sprouse, Preconditioned quantum linear system algorithm, *Phys. Rev. Lett.* **110**, 250504 (2013).
- [6] J. Pan, Y. Cao, X. Yao, Z. Li, C. Ju, H. Chen, X. Peng, S. Kais, and J. Du, Experimental realization of quantum algorithm for solving linear systems of equations, *Phys. Rev. A* **89**, 022313 (2014).
- [7] L. Wossnig, Z. Zhao, and A. Prakash, Quantum linear system algorithm for dense matrices, *Phys. Rev. Lett.* **120**, 050502 (2018).
- [8] J. I. Cirac and P. Zoller, Goals and opportunities in quantum simulation, *Nature Physics* **8**, 264 (2012).
- [9] N. C. Jones, J. D. Whitfield, P. L. McMahon, M.-H. Yung, R. Van Meter, A. Aspuru-Guzik, and Y. Yamamoto, Faster quantum chemistry simulation on fault-tolerant quantum computers, *New Journal of Physics* **14**, 115023 (2012).
- [10] A. A. Houck, H. E. Türeci, and J. Koch, On-chip quantum simulation with superconducting circuits, *Nature Physics* **8**, 292 (2012).
- [11] I. M. Georgescu, S. Ashhab, and F. Nori, Quantum simulation, *Reviews of Modern Physics* **85**, 152 (2013).
- [12] P. J. O’Malley, R. Babbush, I. D. Kivlichan, J. Romero, J. R. McClean, R. Barends, J. Kelly, P. Roushan, A. Tranter, N. Ding, *et al.*, Scalable quantum simulation of molecular energies, *Phys. Rev. X* **6**, 031007 (2016).
- [13] P. W. Shor, Introduction to quantum algorithms, in *Proceedings of Symposia in Applied Mathematics*, Vol. 58 (2002) pp. 143–160.
- [14] A. M. Childs and W. Van Dam, Quantum algorithms for algebraic problems, *Reviews of Modern Physics* **82**, 1 (2010).
- [15] S. E. Venegas-Andraca, Quantum walks: a comprehensive review, *Quantum Information Processing* **11**, 1015 (2012).
- [16] M. Schuld, I. Sinayskiy, and F. Petruccione, An introduction to quantum machine learning, *Contemporary Physics* **56**, 172 (2015).
- [17] A. Montanaro, Quantum algorithms: an overview, *npj Quantum Information* **2**, 1 (2016).
- [18] J. Biamonte, P. Wittek, N. Pancotti, P. Rebentrost, N. Wiebe, and S. Lloyd, Quantum machine learning, *Nature* **549**, 195 (2017).
- [19] J. B. Chang, M. R. Vissers, A. D. Córcoles, M. Sandberg, J. Gao, D. W. Abraham, J. M. Chow, J. M. Gambetta, M. Beth Rothwell, G. A. Keefe, *et al.*, Improved superconducting qubit coherence using titanium nitride, *Applied Physics Letters* **103**, 012602 (2013).
- [20] W. D. Oliver and P. B. Welander, Materials in superconducting quantum bits, *MRS bulletin* **38**, 816 (2013).
- [21] D. Venturelli, M. Do, E. Rieffel, and J. Frank, Compiling quantum circuits to realistic hardware architectures using temporal planners, *Quantum Science and Technology* **3**, 025004 (2018).
- [22] J. Kusyk, S. M. Saeed, and M. U. Uyar, Survey on quantum circuit compilation for noisy intermediate-scale quantum computers: Artificial intelligence to heuristics, *IEEE Transactions on Quantum Engineering* **2**, 1 (2021).
- [23] M. Mergenthaler, C. Müller, M. Ganzhorn, S. Paredes, P. Müller, G. Salis, V. Adiga, M. Brink, M. Sandberg, J. Hertzberg, *et al.*, Effects of surface treatments on flux tunable transmon qubits, *npj Quantum Information* **7**, 1 (2021).
- [24] M. Ban, Photon-echo technique for reducing the decoherence of a quantum bit, *Journal of Modern Optics* **45**, 2315 (1998), <https://doi.org/10.1080/09500349808231241>.
- [25] L. Viola and S. Lloyd, Dynamical suppression of decoherence in two-state quantum systems, *Phys. Rev. A* **58**, 2733 (1998).
- [26] L. Viola, E. Knill, and S. Lloyd, Dynamical decoupling of open quantum systems, *Phys. Rev. Lett.* **82**, 2417 (1999).
- [27] G. A. Paz-Silva and L. Viola, General transfer-function approach to noise filtering in open-loop quantum control, *Phys. Rev. Lett.* **113**, 250501 (2014).
- [28] A. Soare, H. Ball, D. Hayes, J. Sastrawan, M. Jarratt, J. McLoughlin, X. Zhen, T. Green, and M. Biercuk, Experimental noise filtering by quantum control, *Nature Physics* **10**, 825 (2014).
- [29] G. A. Paz-Silva, S.-W. Lee, T. J. Green, and L. Viola, Dynamical decoupling sequences for multi-qubit dephasing suppression and long-time quantum memory, *New Journal of Physics* **18**, 073020 (2016).
- [30] C. L. Edmunds, C. Hempel, R. J. Harris, V. Frey, T. M. Stace, and M. J. Biercuk, Dynamically corrected gates suppressing spatiotemporal error correlations as measured by randomized benchmarking, *Phys. Rev. Research* **2**, 013156 (2020).
- [31] J. Bylander, S. Gustavsson, F. Yan, F. Yoshihara, K. Harrabi, G. Fitch, D. G. Cory, Y. Nakamura, J.-S. Tsia, and W. D. Oliver, Noise spectroscopy through dynamical decoupling with a su-

- perconducting flux qubit, *Nature Physics* **7**, 656 (2019).
- [32] F. Yan, S. Gustavsson, J. Bylander, X. Jin, F. Yoshihara, D. G. Cory, Y. Nakamura, T. P. Orlando, and W. D. Oliver, Rotation-frame relaxation as a noise spectrum analyser of a superconducting qubit undergoing driven evolution, *Nature Communications* **4**, 22337 (2013).
- [33] J. Meeson, A. Ya. Tzalenchuk, and T. Lindström, Evidence for interacting two-level systems from the $1/f$ noise of a superconducting resonator, *Nature Communications* **5**, 4119 (2014).
- [34] C. Müller, J. Lisenfeld, A. Shnirman, and S. Poletto, Interacting two-level defects as sources of fluctuating high-frequency noise in superconducting circuits, *Phys. Rev. B* **92**, 035442 (2015).
- [35] J. J. Burnett, A. Bengtsson, M. Scigliuzzo, D. Niepce, M. Kudra, P. Delsing, and J. Bylander, Decoherence benchmarking of superconducting qubits, *npj Quantum Information* **5**, 54 (2019).
- [36] J. Basset, A. Stockklauser, D.-D. Jarausch, T. Frey, C. Reichl, W. Wegscheider, A. Wallraff, K. Ensslin, and I. T., Evaluating charge noise acting on semiconductor quantum dots in the circuit quantum electrodynamics architecture, *Applied Physics Letters* **105**, 063105 (2014).
- [37] K. W. Chan, W. Huang, C. H. Yang, J. C. C. Hwang, B. Hensen, T. Tanttu, F. E. Hudson, K. M. Itoh, A. Laucht, A. Morello, and A. S. Dzurak, Assessment of a silicon quantum dot spin qubit environment via noise spectroscopy, *Phys. Rev. Applied* **10**, 044017 (2018).
- [38] T. Struck, A. Hollmann, F. Schauer, O. Fedorets, A. Schmidbauer, K. Sawano, H. Riemann, N. V. Abrosimov, L. Cywiński, B. D., and L. R. Schreiber, Low-frequency spin qubit energy splitting noise in highly purified $^{28}\text{Si}/\text{SiGe}$, *npj Quantum Information* **6**, 40 (2020).
- [39] G. A. Álvarez and D. Suter, Measuring the spectrum of colored noise by dynamical decoupling, *Phys. Rev. Lett.* **107**, 230501 (2011).
- [40] L. M. Norris, G. A. Paz-Silva, and L. Viola, Qubit noise spectroscopy for non-gaussian dephasing environments, *Phys. Rev. Lett.* **116**, 150503 (2016).
- [41] P. Szańkowski, G. Ramon, J. Krzywda, D. Kwiatkowski, and L. Cywiński, Environmental noise spectroscopy with qubits subjected to dynamical decoupling, *Journal of Physics: Condensed Matter* **29**, 333001 (2017).
- [42] G. A. Paz-Silva, L. M. Norris, and L. Viola, Multiqubit spectroscopy of gaussian quantum noise, *Phys. Rev. A* **95**, 022121 (2017).
- [43] L. M. Norris, D. Lucarelli, V. M. Frey, S. Mavadia, M. J. Biercuk, and L. Viola, Optimally band-limited spectroscopy of control noise using a qubit sensor, *Phys. Rev. A* **98**, 032315 (2018).
- [44] G. A. Paz-Silva, L. M. Norris, F. Beaudoin, and L. Viola, Extending comb-based spectral estimation to multi-axis quantum noise, *Phys. Rev. A* **100**, 042334 (2019).
- [45] Y. Sung, F. Beaudoin, L. M. Norris, F. Yan, D. K. Kim, J. Y. Qiu, U. von Lüpke, J. L. Yoder, T. P. Orlando, S. Gustavsson, *et al.*, Non-gaussian noise spectroscopy with a superconducting qubit sensor, *Nature communications* **10**, 1 (2019).
- [46] U. von Lüpke, F. Beaudoin, L. M. Norris, Y. Sung, R. Winik, J. Y. Qiu, M. Kjaergaard, D. Kim, J. Yoder, S. Gustavsson, L. Viola, and W. D. Oliver, Two-qubit spectroscopy of spatiotemporally correlated quantum noise in superconducting qubits, *PRX Quantum* **1**, 010305 (2020).
- [47] L. Cywiński, R. M. Lutchyn, C. P. Nave, and S. Das Sarma, How to enhance dephasing time in superconducting qubits, *Phys. Rev. B* **77**, 174509 (2008).
- [48] C. Mullis and L. L. Scharf, Quadratic estimators of the power spectrum, in *Advances in Spectrum Analysis and Array Processing*, edited by S. Haykin (Prentice Hall, Englewood Cliffs, NJ, 1991).
- [49] M. Bartlett and J. Medhi, On the efficiency of procedures for smoothing periodograms from time series with continuous spectra, *Biometrika* **42**, 143 (1955).
- [50] P. Welch, The use of fast fourier transform for the estimation of power spectra: a method based on time averaging over short, modified periodograms, *IEEE Transactions on audio and electroacoustics* **15**, 70 (1967).
- [51] D. J. Thomson, Spectrum estimation and harmonic analysis, *Proceedings of the IEEE* **70**, 1055 (1982).
- [52] S. M. Kay and S. L. Marple, Spectrum analysis—a modern perspective, *Proceedings of the IEEE* **69**, 1380 (1981).
- [53] P. Stoica and R. L. Moses, *Spectral analysis of signals* (Pearson Prentice Hall Upper Saddle River, NJ, 2005).
- [54] G. Udny Yule, On a method of investigating periodicities in disturbed series, with special reference to wolfer's sunspot numbers, *Philosophical Transactions of the Royal Society of London Series A* **226**, 267 (1927).
- [55] G. T. Walker, On periodicity in series of related terms, *Proceedings of the Royal Society of London. Series A, Containing Papers of a Mathematical and Physical Character* **131**, 518 (1931).
- [56] G. E. Box, G. M. Jenkins, G. C. Reinsel, and G. M. Ljung, *Time series analysis: forecasting and control* (John Wiley & Sons, 2015).
- [57] R. Schmidt, Multiple emitter location and signal parameter estimation, *IEEE transactions on antennas and propagation* **34**, 276 (1986).
- [58] K. Schultz, G. Quiroz, P. Titum, and B. Clader, Schwarma: A model-based approach for time-correlated noise in quantum circuits, *Phys. Rev. Research* **3**, 033229 (2021).
- [59] A. Murphy, J. Epstein, G. Quiroz, K. Schultz, L. Tewala, K. McElroy, C. Trout, B. Tien-Street, J. A. Hoffmann, B. Clader, *et al.*, Universal dephasing noise injection via schrodinger wave autoregressive moving average models, *Phys. Rev. Research* **4**, 013081 (2022).
- [60] F. Poggiali, P. Cappellaro, and N. Fabbri, Optimal control for one-qubit quantum sensing, *Phys. Rev. X* **8**, 021059 (2018).
- [61] P. Titum, K. Schultz, A. Seif, G. Quiroz, and B. Clader, Optimal control for quantum detectors, *npj Quantum Information* **7**, 1 (2021).
- [62] C. J. Trout, K. Schultz, P. Titum, L. Norris, G. Quiroz, *et al.*, Provably optimal control for multiplicative amplitude control noise, *arXiv preprint arXiv:2205.06741* (2022).
- [63] A. Schuster, On the investigation of hidden periodicities with application to a supposed 26 day period of meteorological phenomena, *Terrestrial Magnetism* **3**, 13 (1898).
- [64] A. Schuster, The periodogram of magnetic declination as obtained from the records of the greenwich observatory during the years 1871-1895, *Trans. Cambridge Philosophical Soc.* **18**, 107 (1899).
- [65] P. Stoica and Y. Selen, Model-order selection: a review of information criterion rules, *IEEE Signal Processing Magazine* **21**, 36 (2004).
- [66] mezze: a toolox for simulating open quantum system dynamics, <https://github.com/mezze-team/mezze> (2021).
- [67] G. Wilson, Factorization of the covariance generating function of a pure moving average process, *SIAM Journal on Numerical Analysis* **6**, 1 (1969).
- [68] S.-P. Wu, S. Boyd, and L. Vandenberghe, Fir filter design via spectral factorization and convex optimization, in *Applied and computational control, signals, and circuits* (Springer, 1999) pp. 215–245.
- [69] A. Kaderli and A. S. Kayhan, Spectral estimation of arma processes using arma-cepstrum recursion, *IEEE Signal Processing*

- Letters **7**, 259 (2000).
- [70] V. F. Pisarenko, The retrieval of harmonics from a covariance function, *Geophysical Journal International* **33**, 347 (1973).
- [71] M. Abadi, A. Agarwal, P. Barham, E. Brevdo, Z. Chen, C. Citro, G. S. Corrado, A. Davis, J. Dean, M. Devin, S. Ghemawat, I. Goodfellow, A. Harp, G. Irving, M. Isard, Y. Jia, R. Jozefowicz, L. Kaiser, M. Kudlur, J. Levenberg, D. Mané, R. Monga, S. Moore, D. Murray, C. Olah, M. Schuster, J. Shlens, B. Steiner, I. Sutskever, K. Talwar, P. Tucker, V. Vanhoucke, V. Vasudevan, F. Viégas, O. Vinyals, P. Warden, M. Wattenberg, M. Wicke, Y. Yu, and X. Zheng, [TensorFlow: Large-scale machine learning on heterogeneous systems](#) (2015), software available from tensorflow.org.
- [72] D. P. Kingma and J. Ba, Adam: A method for stochastic optimization, arXiv preprint arXiv:1412.6980 (2014).
- [73] K. Schultz, R. LaRose, A. Mari, G. Quiroz, N. Shammah, B. D. Clader, and W. J. Zeng, Reducing the impact of time-correlated noise on zero-noise extrapolation, arXiv preprint arXiv:2201.11792 (2022).
- [74] E. Knill, D. Leibfried, R. Reichle, J. Britton, R. B. Blakestad, J. D. Jost, C. Langer, R. Ozeri, S. Seidelin, and D. J. Wineland, Randomized benchmarking of quantum gates, *Phys. Rev. A* **77**, 012307 (2008).
- [75] E. Nielsen, J. K. Gamble, K. Rudinger, T. Scholten, K. Young, and R. Blume-Kohout, Gate Set Tomography, *Quantum* **5**, 557 (2021).
- [76] V. Ingle, S. Kogon, and D. Manolakis, *Statistical and adaptive signal processing* (Artech, 2005).